Gate-tunable supercurrent and multiple Andreev reflections in a superconductor-topological insulator nanoribbon-superconductor hybrid device

Luis A. Jauregui,[1,a),b)] Morteza Kayyalha,[1,a)] Aleksandr Kazakov,[2] Ireneusz Miotkowski,[2] Leonid P. Rokhinson,[1,2] and Yong P. Chen[1,2,3,4,c)]
[1]*School of Electrical and Computer Engineering and Birck Nanotechnology Center, Purdue University, West Lafayette, Indiana 47907, USA*
[2]*Department of Physics and Astronomy, Purdue University, West Lafayette, Indiana 47907, USA*
[3]*Purdue Quantum Center, Purdue University, West Lafayette, Indiana 47907, USA*
[4]*WPI-AIMR International Research Center on Materials Sciences, Tohoku University, Sendai 980-8577, Japan*

(Received 9 October 2017; accepted 11 February 2018; published online 27 February 2018)

We report on the observation of gate-tunable proximity-induced superconductivity and multiple Andreev reflections (MARs) in a bulk-insulating $BiSbTeSe_2$ topological insulator nanoribbon (TINR) Josephson junction with superconducting Nb contacts. We observe a gate-tunable critical current (I_C) for gate voltages (V_g) above the charge neutrality point (V_{CNP}), with I_C as large as 430 nA. We also observe MAR peaks in the differential conductance (dI/dV) versus DC voltage (V_{dc}) across the junction corresponding to sub-harmonic peaks (at $V_{dc} = V_n = 2\Delta_{Nb}/en$, where Δ_{Nb} is the superconducting gap of the Nb contacts and n is the sub-harmonic order). The sub-harmonic order, n, exhibits a V_g-dependence and reaches $n = 13$ for $V_g = 40$ V, indicating the high transparency of the Nb contacts to TINR. Our observations pave the way toward exploring the possibilities of using TINR in topologically protected devices that may host exotic physics such as Majorana fermions. *Published by AIP Publishing.* https://doi.org/10.1063/1.5008746

Three-dimensional topological insulators (TIs) are a new class of quantum matter with insulating bulk and conducting surface states, topologically protected against time-reversal-invariant perturbations (scattering by non-magnetic impurities such as crystalline defects and surface roughness).[1,2] Topological superconductors (TSCs) are another important class of quantum matter and are analogous to TIs, where the superconducting gap and Majorana fermions of TSCs replace the bulk bandgap and Dirac fermion surface states of the TI, respectively.[2] Controlling the Majorana modes is considered one of the important approaches for developing topologically protected quantum computers. Three-dimensional (3D) TIs in proximity to s-wave superconductors have been proposed as one of the promising platforms to realize topological superconductivity and Majorana fermions.[3] In this context, it has been pointed out that TI nanowires (TINWs) possess various appealing features for such studies.[4–8] However, the first important step is to understand how TI nanowires, including nanoribbons (TINRs), behave in contact with superconducting leads.

Superconductor-normal-superconductor (SNS) Josephson junctions (JJs), with topological insulators as the normal material, have been experimentally realized on 3D-TIs.[9–22] However, TI materials used in many of the previous experiments have notable bulk conduction, making it challenging to distinguish from the contribution of the topological surface states. In this letter, we study S-TINR-S Josephson junctions, where S = Niobium (Nb) and the TINRs are mechanically exfoliated from bulk $BiSbTeSe_2$ (BSTS) TI crystals. Our BSTS is among the most bulk-insulating TIs with surface state dominated conduction and chemical potential located close to the surface state Dirac point in the bulk bandgap.[23,24] Therefore, our study enables us to investigate the proximity effects and induced superconductivity in such "intrinsic" (bulk-insulating) and gate-tunable TINRs with both electron (n) and hole (p) dominated surface transport. Moreover, we are able to investigate the transparency of our superconducting contacts to TINRs both in n- and p-dominated transport regimes through the observation of multiple Andreev reflections (MARs).

High-quality single crystals of BSTS were grown by the Bridgman technique as described elsewhere.[23,24] Devices fabricated on the exfoliated flakes from these crystals exhibit surface dominated conduction with ambipolar field effects, half-integer quantum hall effects, and π Berry's phase.[23,24] We obtain BSTS nanoribbons using a standard mechanical exfoliation technique and transfer them onto a 500-μm thick highly doped Si substrate (used as the back gate) covered with 300-nm SiO_2 on top. We locate BSTS nanoribbons, which are randomly dispersed on the substrate, using an optical microscope. An atomic force microscopy (AFM) image of a representative JJ is shown in Fig. 1(a). Multiple electrodes, with electrode separation $L < 100$ nm between the adjacent electrodes, are defined by e-beam lithography for each TINR. We then deposit 30-nm thick Nb contacts by a DC sputtering system. A short (~5 s) *in situ* Ar ion milling prior to the metal deposition is used to remove any residues left from the lithography step and native oxides on the TINR surface. Our results presented here are taken from a TINR

[a)]L. A. Jauregui and M. Kayyalha contributed equally to this work.
[b)]Present address: Department of Physics, Harvard University, Cambridge, MA 02138, USA.
[c)]Electronic mail: yongchen@purdue.edu

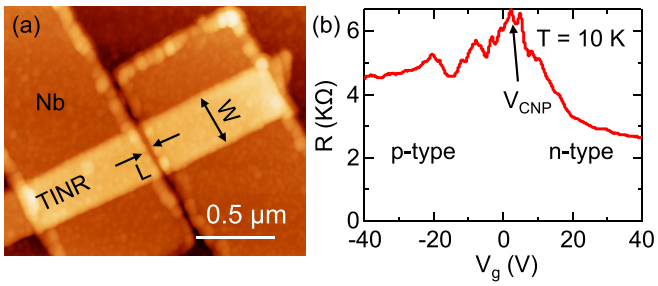

FIG. 1. (a) Atomic force microscopy (AFM) image of a 250-nm wide and 20-nm thick TINR multi-terminal device with Nb electrodes (electrode separation L ~ 60 nm). (b) Two-terminal resistance (R) vs. the back-gate voltage (V_g), measured at $T = 10$ K, above the critical temperature (T_C^{Nb}) of the Nb electrodes.

sample with a thickness of ~20 nm, a width of ~250 nm, and an electrode separation of ~60 nm.

Figure 1(b) depicts R vs. the back-gate voltage (V_g) at $T = 10$ K (above the critical temperature of our deposited superconductor, $T_C^{Nb} \sim 6.5$ K). The charge neutrality-point voltage (V_{CNP}) is ~4 V for this device. The electron- and hole-dominated regimes can be easily observed in Fig. 1(b) as we tune V_g away from V_{CNP}. Using BCS theory, we estimate the $T = 0$ K superconducting gap as $\Delta_{Nb} = 1.76 k_B T_C^{Nb} \sim 975\ \mu$eV.

When the sample is cooled down below T_C^{Nb}, the electronic transport in the junction is strongly affected by the superconducting proximity effect. The evidences of this effect manifest themselves as the flow of a supercurrent in the junction and the appearance of multiple Andreev reflections (MARs).[25,26] Figure 2(a) shows the colormap of the differential resistance (dV/dI) vs. V_g and I_{dc} at $T = 30$ mK. The DC voltage vs. current (V_{dc} vs. I_{dc}) characteristic of the junction at $T = 30$ mK for a few different V_g's is also presented in Fig. 2(b). As we increase I_{dc} from zero, the junction is in its superconducting state and its resistance is zero. However, once I_{dc} is increased above a critical value [I_C, marked by an arrow in Fig. 2(b)], the junction transitions from the superconducting state to a normal state with a non-zero resistance. The junction critical current, I_C, is highlighted by a white curve in Fig. 2(a). First, we observe that I_C is gate tunable, with larger I_C for $V_g > V_{CNP}$. However, when V_g is tuned near the charge neutrality point ($V_{CNP} \sim 4$ V), I_C decreases and eventually saturates for more negative V_g's as previously observed in Bi_2Se_3 flakes[27] and graphene.[28,29] One possible explanation for the saturation of I_C for V_g below V_{CNP} is that the Nb electrodes electron-dope the underlying material (TINR). Therefore, when $V_g < V_{CNP}$, a p-n junction is formed in the TINR. This p-n junction can weaken and eventually break the induced superconductivity as was shown in graphene.[30] Furthermore, despite that the total charge of the system is neutral close to the CNP, the top and bottom surfaces may be oppositely charged due to the difference in their coupling to the back gate. This charge inhomogeneity may also contribute to the saturation of I_C for $V_g \leq V_{CNP}$. Another plausible explanation may be the poor injection of the holes into TINRs by Nb, as will be demonstrated from the low transparency of the contacts for $V_g < V_{CNP}$ from our analysis of MARs (Fig. 3). The inset of Fig. 2(b) shows the dependence of I_C on the Fermi momentum (k_F), where $k_F = \sqrt{4\pi C_{ox}(V_g - V_{CNP})/e}$ and C_{ox} is the parallel plate capacitance per unit area of 300-nm SiO_2 (~12 nF/cm^2). For $k_F > 0.4$ nm^{-1}, we observe that I_C varies linearly with k_F, as experimentally demonstrated in ballistic graphene Josephson junctions.[31] The measured mean free path of BSTS flakes is ~100 nm.[23,24] Given the channel length $L \sim 60$ nm, we believe our junctions to be in the ballistic limit, corroborating the linear dependence of I_C with k_F. We also observe that the junction critical temperature (T_C, the temperature below which the junction resistance goes to zero and supercurrent starts to flow in the junction) changes with V_g from $T_C = 1.6$ K for $V_g = 40$ V to $T_C = 0.7$ K for $V_g = 10$ V. Using BCS theory, we extract the induced superconducting gap (Δ) in the TINR as $\Delta = 1.76 k_B T_C = 242\ \mu$eV and 106 μeV for $V_g = 40$ V and $V_g = 10$ V, respectively. The superconducting coherence length ($\xi = \hbar v_F/\pi\Delta$) varies from 600 nm to 260 nm for $V_g = 10$ and 40 V, respectively. We note that the resistance (dV/dI) of the junction does not change as we increase V_{dc} above Δ_{Nb}/e (~975 μV) and even slightly beyond $2\Delta_{Nb}/e$ as will be discussed later. As a result, the normal resistance (R_N) in our junctions is obtained at V_{dc} slightly above Δ_{Nb}/e. We obtain $I_C R_N \sim 304\ \mu$V and 266 μV for $V_g = 40$ V and 10 V, respectively. Such large $I_C R_N$ products (compared to Δ) again point towards the ballistic nature of superconducting transport in our sample as recently reported in other TI junctions.[32]

Figure 3(a) displays dI/dV vs. V_{dc} for $V_g = 40$ V at $T = 30$ mK. Several peaks (within the Nb superconducting gap) in dI/dV are observed at $V_{dc} = V_n = 2\Delta_{Nb}/en$ (where $n = 2$, 3, 4, 5, 6, 9, and 13) as marked by the arrows in

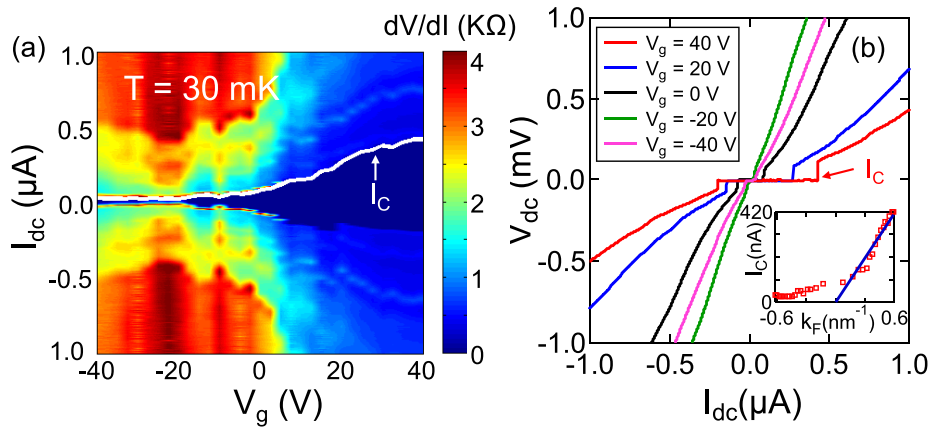

FIG. 2. (a) Color map of dV/dI vs. V_g and bias current I_{dc} for $T = 30$ mK. Critical current (I_C) is represented by a white trace on the colormap. (b) DC voltage (V_{dc}) vs. DC current (I_{dc}) characteristic of the device for different V_g's at $T = 30$ mK. Inset: I_C vs. k_F (Fermi momentum). The blue curve is a linear fit for $k_F > 0.4$ nm^{-1}. Data in (a) and (b) were measured with sweeping I_{dc} from -1 μA to 1 μA.

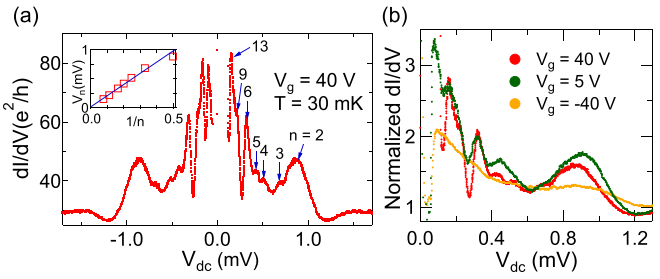

FIG. 3. (a) Differential conductance (dI/dV) vs. V_{dc} for $V_g = 40$ V. Each dI/dV peak position (V_n, expected to be $2\Delta_{Nb}/en$) is labeled with its index n, starting with $n = 2$ for the peak near $V_{dc} = 900$ μeV. Inset: V_n vs. $1/n$. The solid line is a linear fit with a corresponding slope of ~1.8 meV, which agrees with $2\Delta_{Nb}$ calculated from the BCS theory for the observed junction critical temperature $T_C \sim 6.5$ K. (b) dI/dV normalized by $1/R_N$ vs. V_{dc} for three representative V_g's = 40, −40, and 5 V, corresponding to n-type and p-type and near the charge neutrality point. All the measurements were performed at $T = 30$ mK.

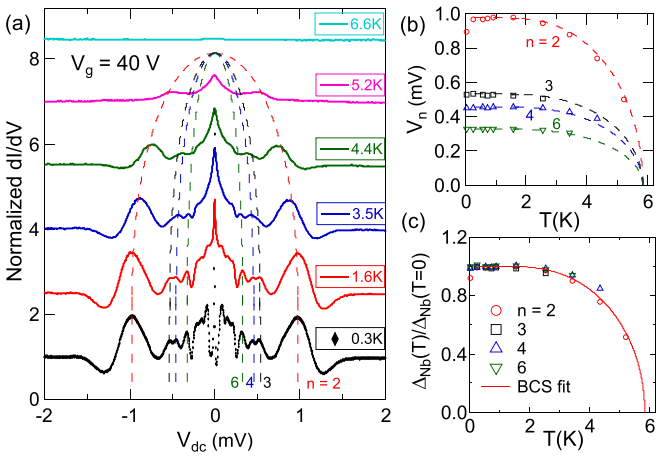

FIG. 4. (a) Normalized dI/dV vs. V_{dc} for different Ts at $V_g = 40$ V. Dashed lines are guides to the eye corresponding to the expected T-dependence of V_n from BCS theory for $n = 2$, 3, 4, and 6. (b) V_n vs. T for $n = 2$, 3, 4, and 6. Dashed lines are BCS fits. (c) Temperature dependence of normalized $\Delta_{Nb}/\Delta_{Nb}(T = 0\,K)$, where $\Delta_{Nb} = enV_n(T)/2$ is obtained from different dI/dV peaks corresponding to $n = 2$, 3, 4, and 6. The solid line is a BCS-theory fit.

Fig. 3(a). These dI/dV peaks are consistent with MARs.[25] We note that these peaks are symmetric around $V_{dc} = 0$ V, and thus, below we focus only on the positive peaks. No feature in dI/dV vs. V_{dc} is identified for $n = 1$, and R_N is achieved for $V > \Delta_{Nb}/e$ instead of $V > 2\Delta_{Nb}/e$. The absence of the first ($n = 1$) MAR peak has been noted in some SNS junctions[20,26] and may be related to the presence of mid-gap zero-energy states as described elsewhere.[33,34] From the linear fit of dI/dV peaks vs. $1/n$, we obtain $\Delta_{Nb} \sim 900$ μeV, which is in excellent agreement with Δ_{Nb} obtained from the BCS theory and $T_C^{Nb} \sim 6.5$ K. Moreover, the observed dI/dV peaks are reproducible and independent of the V_{dc} sweep direction. While we do not observe any dI/dV peaks corresponding to $n = 7$ and 8, higher-order peaks ($n = 9$ and 13) are present, a feature that has been previously observed[26] and requires further investigation. The observation of the high-order MAR peaks is an indication of high transparency of contacts in our junction.

Figure 3(b) depicts the differential conductance (dI/dV, normalized by $1/R_N$) vs. (positive) V_{dc} for T = 30 mK at three different V_g's. First, we observe that the position of the dI/dV peaks remains relatively constant with V_g, in contrast to the oscillatory behavior of dI/dV peaks around a resonant level in a quantum dot.[35,36] This suggests the absence of localized states in our TINR devices. The high-order dI/dV peaks observed for $V_g > V_{CNP}$ further indicate that the contacts are highly transparent. Even though the large $I_C R_N$ product and the linear dependence of I_C vs. k_F point towards the ballistic nature of transport, the small amplitude of MAR peaks [as shown in Fig. 3(b)] has been previously attributed to a diffusive transport regime in graphene JJs.[37] Such discrepancies require further investigations. For $V_g < V_{CNP}$, the amplitude of the dI/dV peaks decreases with more negative V_g, e.g., with vanishing peak amplitudes for $n = 3$, 4, 5, 6, and 9 at $V_g = -40$ V. The vanishing of dI/dV peaks for $V_g < V_{CNP}$ may be related to the pinning of the Fermi level to the electron-doped regime under the Nb electrodes and hence the formation of p-n junctions for $V_g < V_{DP}$, where V_{DP} is the Dirac point voltage, as has been observed in graphene JJs.[28,29]

Figure 4(a) depicts the T-dependence of dI/dV (normalized by $1/R_N$) vs. V_{dc} for $V_g = 40$ V, exhibiting a reduction of the Nb superconducting gap with increasing T. Dashed lines are guides to the eye corresponding to the expected T-dependence of dI/dV peak positions (V_n) from BCS theory. We observe a nearly flat and featureless dI/dV vs. V_{dc} for T = 6.6 K (slightly above $T_C^{Nb} \sim 6.5$ K). We also observe that while dI/dV peaks are noticeable up to high temperatures (~5.2 K), the amplitude of the peaks reduces with increasing T, and some of the peaks merge together at higher T (e.g., peaks for $n = 3$ and 4 merge at T = 3.5 K). Figure 4(b) shows the T-dependence of V_n for $n = 2$, 3, 4, and 6. Using the BCS theory to fit V_n vs. T, we extract $T_C \sim 6$ K, in fair agreement with $T_C^{Nb} \sim 6.5$ K. Figure 4(c) displays the T-dependence of Δ_{Nb} extracted from each dI/dV peak (for $n = 2$, 3, 4, and 6), where $\Delta_{Nb} = neV_n(T)/2$, together with the fit of Δ_{Nb} vs. T obtained from the BCS theory, which is seen to describe the data well.

We demonstrated Josephson junctions based on mechanically exfoliated bulk-insulating 3D topological insulator nanoribbons in proximity to superconducting Nb electrodes. We observe high-order ($n = 13$) multiple Andreev reflections, demonstrating that charge transport in the TINR channel is coherent. Furthermore, the critical current exhibits gate effects and can be gate-tuned around one order of magnitude from ~50 nA to ~430 nA at 30 mK. Our measurements of supercurrent in Josephson junctions based on TINRs help to better understand the nature of induced superconductivity in these junctions and pave the way toward exploration of the envisioned topologically protected devices based on superconductor-TINR-superconductor junctions.

We acknowledge support from NSF (DMR No. 1410942). The TI material synthesis was supported by the DARPA MESO Program (Grant No. N66001-11-1-4107). L.A.J. also acknowledges support from a Purdue Center for Topological Materials fellowship. L.P.R. and A.K. acknowledge support from the U.S. Department of Energy under Award No. DE-SC0008630.

[1]M. Z. Hasan and C. L. Kane, "Colloquium: Topological insulators," Rev. Mod. Phys. **82**, 3045–3067 (2010).

[2]X.-L. Qi and S.-C. Zhang, "Topological insulators and superconductors," Rev. Mod. Phys. **83**, 1057–1110 (2011).
[3]L. Fu and C. L. Kane, "Superconducting proximity effect and Majorana fermions at the surface of a topological insulator," Phys. Rev. Lett. **100**, 096407 (2008).
[4]A. Cook and M. Franz, "Majorana fermions in a topological-insulator nanowire proximity-coupled to an s-wave superconductor," Phys. Rev. B **84**, 201105 (2011).
[5]A. M. Cook, M. M. Vazfeh, and M. Franz, "Stability of Majorana fermions in proximity-coupled topological insulator nanowires," Phys. Rev. B **86**, 155431 (2012).
[6]R. Ilan, J. H. Bardarson, H. S. Sim, and J. E. Moore, "Detecting perfect transmission in Josephson junctions on the surface of three dimensional topological insulators," New J. Phys. **16**, 053007 (2014).
[7]L. A. Jauregui, M. T. Pettes, L. P. Rokhinson, L. Shi, and Y. P. Chen, "Gate tunable relativistic mass and Berry's phase in topological insulator nanoribbon field effect devices," Sci. Rep. **5**, 8452 (2015).
[8]L. A. Jauregui, M. T. Pettes, L. P. Rokhinson, L. Shi, and Y. P. Chen, "Magnetic field-induced helical mode and topological transitions in a topological insulator nanoribbon," Nat. Nanotechnol. **11**, 345–351 (2016).
[9]B. Sacépé, J. B. Oostinga, J. Li, A. Ubaldini, N. J. Couto, E. Giannini, and A. F. Morpurgo, "Gate-tuned normal and superconducting transport at the surface of a topological insulator," Nat. Commun. **2**, 575 (2011).
[10]F. Qu, F. Yang, J. Shen, Y. Ding, J. Chen, Z. Ji, G. Liu, J. Fan, X. Jing, C. Yang, and L. Lu, "Strong superconducting proximity effect in Pb-Bi_2Te_3 hybrid structures," Sci. Rep. **2**, 339 (2012).
[11]M. Veldhorst, M. Snelder, M. Hoek, T. Gang, V. K. Guduru, X. L. Wang, U. Zeitler, W. G. van der Wiel, A. A. Golubov, H. Hilgenkamp, A. Brinkman, V. K. Guduru, U. Zeitler, W. G. van der Wiel, A. A. Golubov, H. Hilgenkamp, and A. Brinkman, "Josephson supercurrent through a topological insulator surface state," Nat. Mater. **11**, 417–421 (2012).
[12]J. R. Williams, A. J. Bestwick, P. Gallagher, S. S. Hong, Y. Cui, A. S. Bleich, J. G. Analytis, I. R. Fisher, and D. Goldhaber-Gordon, "Unconventional Josephson effect in hybrid superconductor-topological insulator devices," Phys. Rev. Lett. **109**, 056803 (2012).
[13]I. Sochnikov, A. J. Bestwick, J. R. Williams, T. M. Lippman, I. R. Fisher, D. Goldhaber-Gordon, J. R. Kirtley, and K. A. Moler, "Direct measurement of current-phase relations in superconductor/topological insulator/superconductor junctions," Nano Lett. **13**, 3086–3092 (2013).
[14]J. B. Oostinga, L. Maier, P. Schüffelgen, D. Knott, C. Ames, C. Brüne, G. Tkachov, H. Buhmann, and L. W. Molenkamp, "Josephson supercurrent through the topological surface states of strained bulk HgTe," Phys. Rev. X **3**, 021007 (2013).
[15]A. D. K. Finck, C. Kurter, Y. S. Hor, and D. J. V. Harlingen, "Phase coherence and Andreev reflection in topological insulator devices," Phys. Rev. X **4**, 041022 (2014).
[16]J. H. Lee, G.-H. Lee, J. Park, J. Lee, S.-G. Nam, Y.-S. Shin, J. S. Kim, and H.-J. Lee, "Local and nonlocal Fraunhofer-like pattern from an edge-stepped topological surface Josephson current distribution," Nano Lett. **14**, 5029–5034 (2014).
[17]L. Yang, X. Cui, J. Zhang, K. Wang, M. Shen, S. Zeng, S. A. Dayeh, L. Feng, and B. Xiang, "Lattice strain effects on the optical properties of MoS2 nanosheets," Sci. Rep. **4**, 5649 (2014).
[18]D. Zhang, J. Wang, A. M. Dasilva, J. S. Lee, H. R. Gutierrez, M. H. W. Chan, J. Jain, and N. Samarth, "Superconducting proximity effect and possible evidence for Pearl vortices in a candidate topological insulator," Phys. Rev. B **84**, 161520 (2011).
[19]C. Kurter, A. D. K. Finck, Y. S. Hor, and D. J. Van Harlingen, "Evidence for an anomalous current-phase relation in topological insulator Josephson junctions," Nat. Commun. **6**, 7130 (2015).
[20]J. Wiedenmann, E. Bocquillon, R. S. Deacon, S. Hartinger, O. Herrmann, T. M. Klapwijk, L. Maier, C. Ames, C. Brüne, C. Gould, A. Oiwa, K. Ishibashi, S. Tarucha, H. Buhmann, and L. W. Molenkamp, "4π-periodic Josephson supercurrent in HgTe-based topological Josephson junctions," Nat. Commun. **7**, 10303 (2016).
[21]M. P. Stehno, V. Orlyanchik, C. D. Nugroho, P. Ghaemi, M. Brahlek, N. Koirala, S. Oh, and D. J. V. Harlingen, "Signature of a topological phase transition in the Josephson supercurrent through a topological insulator," Phys. Rev. B **93**, 035307 (2016).
[22]R. S. Deacon, J. Wiedenmann, E. Bocquillon, F. Domínguez, T. M. Klapwijk, P. Leubner, C. Brüne, E. M. Hankiewicz, S. Tarucha, K. Ishibashi, H. Buhmann, and L. W. Molenkamp, "Josephson radiation from gapless Andreev bound states in HgTe-based topological junctions," Phys. Rev. X **7**, 021011 (2017).
[23]Y. Xu, I. Miotkowski, C. Liu, J. Tian, H. Nam, N. Alidoust, J. Hu, C.-K. Shih, M. Z. Hasan, and Y. P. Chen, "Observation of topological surface state quantum Hall effect in an intrinsic three-dimensional topological insulator," Nat. Phys. **10**, 956–963 (2014).
[24]Y. Xu, I. Miotkowski, and Y. P. Chen, "Quantum transport of two-species Dirac fermions in dual-gated three-dimensional topological insulators," Nat. Commun. **7**, 11434 (2016).
[25]M. Tinkham, *Introduction to Superconductivity* (Dover Publications, 2004), p. 454.
[26]J. Xiang, A. Vidan, M. Tinkham, R. M. Westervelt, and C. M. Lieber, "Ge/Si nanowire mesoscopic Josephson junctions," Nat. Nanotechnol. **1**, 208–213 (2006).
[27]S. Cho, B. Dellabetta, A. Yang, J. Schneeloch, Z. Xu, T. Valla, G. Gu, M. J. Gilbert, and N. Mason, "Symmetry protected Josephson supercurrents in three-dimensional topological insulators," Nat. Commun. **4**, 1689 (2013).
[28]M. Ben Shalom, M. J. Zhu, V. I. Fal'ko, A. Mishchenko, A. V. Kretinin, K. S. Novoselov, C. R. Woods, K. Watanabe, T. Taniguchi, A. K. Geim, and J. R. Prance, "Quantum oscillations of the critical current and high-field superconducting proximity in ballistic graphene," Nat. Phys. **12**, 318–322 (2016).
[29]V. E. Calado, S. Goswami, G. Nanda, M. Diez, A. R. Akhmerov, K. Watanabe, T. Taniguchi, T. M. Klapwijk, and L. M. K. Vandersypen, "Ballistic Josephson junctions in edge-contacted graphene," Nat. Nanotechnol. **10**, 761–765 (2015).
[30]J.-H. Choi, G.-H. Lee, S. Park, D. Jeong, J.-O. Lee, H.-S. Sim, Y.-J. Doh, and H.-J. Lee, "Complete gate control of supercurrent in graphene p-n junctions," Nat. Commun. **4**, 2525 (2013).
[31]N. Mizuno, B. Nielsen, and X. Du, "Ballistic-like supercurrent in suspended graphene Josephson weak links," Nat. Commun. **4**, 2716 (2013).
[32]P. Schüffelgen, D. Rosenbach, C. Li, T. Schmitt, M. Schleenvoigt, A. R. Jalil, J. Kölzer, M. Wang, B. Bennemann, U. Parlak *et al*., "Boosting transparency in topological josephson junctions via stencil lithography," preprint arXiv:1711.01665 (2017).
[33]D. M. Badiane, M. Houzet, and J. S. Meyer, "Nonequilibrium Josephson effect through helical edge states," Phys. Rev. Lett. **107**, 177002 (2011).
[34]P. San-Jose, J. Cayao, E. Prada, and R. Aguado, "Multiple Andreev reflection and critical current in topological superconducting nanowire junctions," New J. Phys. **15**, 075019 (2013).
[35]M. R. Buitelaar, W. Belzig, T. Nussbaumer, B. Babić, C. Bruder, and C. Schönenberger, "Multiple Andreev reflections in a carbon nanotube quantum dot," Phys. Rev. Lett. **91**, 057005 (2003).
[36]P. Jarillo-Herrero, J. A. van Dam, and L. P. Kouwenhoven, "Quantum supercurrent transistors in carbon nanotubes," Nature **439**, 953–956 (2006).
[37]X. Du, I. Skachko, and E. Y. Andrei, "Josephson current and multiple Andreev reflections in graphene SNS junctions," Phys. Rev. B **77**, 184507 (2008).